

On a PDE-based material parameter identification problem with contact constraints

Simon Hubmer¹, Stefan Kindermann², Ekaterina Sherina^{3,4}

May 12, 2026

Abstract

We consider the identification of a scalar coefficient in a PDE-based parameter estimation problem with contact constraints. The considered problem can be used as an idealized model of a membrane under forces, constrained by a barrier or indenter. More generally, it serves as a benchmark for the analysis of more complex contact problems and the development of corresponding reconstruction algorithms. In this paper, we discuss both the forward and inverse parameter estimation problems, as well as uniqueness and non-uniqueness issues caused by the contact constraints. Furthermore, we consider the design and implementation of reconstruction approaches which we test on numerical examples, illustrating both uniqueness and non-uniqueness as well as parameter identifiability.

Keywords. Inverse and Ill-Posed Problems, Material Parameter Estimation, Contact Constraints, Membrane Coefficient Estimation, Iterative Regularization

1 Introduction

In this paper, we consider the estimation of the scalar coefficient a in the constrained PDE

$$\begin{aligned} -\operatorname{div}(a(x)\nabla u(x)) &= f(x), & \forall x \in \Omega \cap \{u > h\}, \\ u(x) &\geq h(x), & \text{a.e. in } \Omega, \end{aligned} \tag{1.1}$$

augmented with boundary conditions (e.g., $u = 0$ on $\partial\Omega$), where Ω is a bounded Lipschitz domain, the functions f and h are known, and direct or indirect measurements

¹Johannes Kepler University Linz, Institute of Industrial Mathematics, Altenbergerstraße 69, A-4040 Linz, Austria, (simon.hubmer@jku.at)

²Johannes Kepler University Linz, Institute of Industrial Mathematics, Altenbergerstraße 69, A-4040 Linz, Austria, (kindermann@indmath.uni-linz.ac.at)

³University of Vienna, Faculty of Mathematics, Oskar Morgenstern-Platz 1, 1090 Vienna, Austria (ekaterina.sherina@univie.ac.at), **corresponding author**

⁴Christian Doppler Laboratory for Mathematical Modeling and Simulation of Next Generations of Ultrasound Devices (MaMSi), Oskar Morgenstern-Platz 1, 1090 Vienna, Austria

of u are available up to a certain amount of measurement noise. We furthermore assume in the following that $0 < c_1 < a(x) < c_2$, a.e. in Ω with positive constants $c_1, c_2 \in \mathbb{R}$.

Without the constraint $u \geq h$, this is a standard parameter estimation problem for PDEs and has been studied extensively in the past, both theoretically and numerically, for example, within the context of the inverse conductivity problem [11, 41], electrical impedance tomography [13, 37, 54], or acousto-electrical tomography [2, 5, 12, 38, 64].

However, less is known about the parameter identification in the setting (1.1) with constraints. The model problem (1.1) can be seen as an idealized model of a membrane under forces, where the (contact) constraint $u \geq h$ models a barrier or an indenter with the shape h . As such, it serves as a simplified model of an indentation test in elasticity/elastography. Here, the coefficient a might represent an elasticity or geometric (thickness) parameter of the membrane, and the goal is to identify it from (partial knowledge) of the deformation. Furthermore, (1.1) can also be seen as a general benchmark problem for the analysis of material parameter estimation problems with more complex contact conditions, such as the Signorini conditions [50], and for the development of corresponding reconstruction approaches.

In contrast to the problem without constraints, we found that the coefficient-inverse problem for (1.1) (or related constraint problems) was comparatively scarcely studied in the literature: Parameters (both elastic ones and others) were identified mostly by using variants of an output-least squares fitting, e.g., in [9, 53, 60, 62]; the parameter identification for a 1D beam model was investigated in [56]. Furthermore, the identification of elastic parameters from indentation curves has been studied in [19, 63] (see also the informative review [10]); finally, a parametric identification problem for indentation problems was considered in [22]. On a more abstract level, related to our model problem, there is considerable literature for inverse problems for variational inequalities, e.g., the comprehensive work of [30–33, 42, 49]. These results are broad extensions of the abstract energy-functional (variational) approach for elliptic parameter identification problems (see, e.g., [27–29]) to the contact case. Note that our work has a slightly different focus than these works in that we from the outset consider the case of partial observations and also investigate iterative (and not necessarily variational) methods for solving the inverse problem.

Hence, in this paper we study both the forward and inverse problems corresponding to the constrained PDE model (1.1) and discuss questions of uniqueness and non-uniqueness in relation to the contact condition $u \geq h$, as well as some aspects of the corresponding regularization and reconstruction algorithms. In contrast to the classic inverse conductivity problem, non-uniqueness can be seen to occur due to the presence and shape of the indenter, which can also be understood intuitively within the viewpoint of a constrained membrane under forces. Furthermore, we consider the stable recovery of the parameter a using (iterative) regularization methods in both finite and infinite dimensional settings. These are adapted to the non-differential nature of the underlying problem, requiring suitable approximation techniques. Finally, we conduct a number of numerical experiments on simulated data to illustrate the challenges of the problem, and to demonstrate the performance of the proposed reconstruction algorithms.

The outline of this paper is as follows: In Section 2 and Section 3 we study the

forward and inverse contact problem, respectively, and consider uniqueness and non-uniqueness caused by the contact constraints. In Section 4, we consider regularization approaches for the inverse contact problems, and in Section 5 discuss the discretization of both the forward and inverse problems. Finally, in Section 6, we provide a number of illustrative numerical examples, and finish with a brief conclusion in Section 7.

2 The forward contact problem

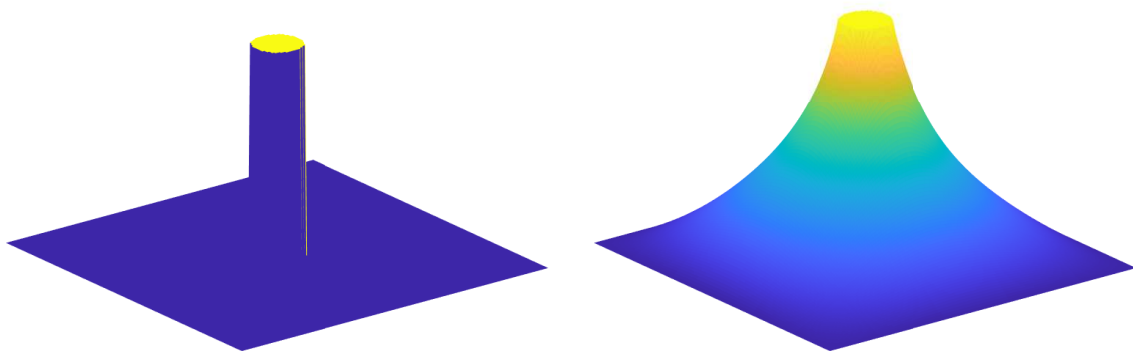


Figure 2.1: Illustrative example of a constraint function (= indenter shape) $h(x)$ (left) and corresponding solution of the forward contact problem (2.1) (right).

In this section, we consider the mathematically rigorous formulation of our model problem (1.1) for u , and discuss a number of equivalent variants used below.

For this, we start by reformulating the problem as a constraint energy minimization problem in appropriate Hilbert spaces for given a (and f, h and, for simplicity, using homogeneous Dirichlet conditions on the boundary): The solution u is defined by

$$u := \arg \min_{v \in H_0^1(\Omega)} \frac{1}{2} \int_{\Omega} a(x) |\nabla v(x)|^2 dx - \int_{\Omega} f(x)v(x) dx, \quad (2.1)$$

s.t. $v(x) \geq h(x)$ a.e. in Ω .

Figure 2.1 illustrates an instance of h and the corresponding solution u . Intuitively, it is clear that the optimality conditions for the minimization problem in (2.1) lead to the equations in (1.1), and for the remainder of the paper, we thus use (2.1) as the (rigorous) definition of our model problem. Note that an alternative treatment of, e.g., Neumann boundary conditions could be pursued along similar lines.

First, we show that (2.1) has a unique solution under standard assumptions. For this, we start by expressing the constraint $v \geq h$ as $v \in K_h$, where

$$K_h := \{v \in H_0^1(\Omega) \mid v(x) \geq h(x) \text{ a.e. in } \Omega\}. \quad (2.2)$$

With this definition, we obtain the following characterization:

Lemma 2.1. *For $h \in H_0^1(\Omega)$ the set K_h defined in (2.2) is closed. Furthermore,*

$$K_h = h + K_0,$$

and K_0 is a closed convex nonempty cone in $H_0^1(\Omega)$.

Proof. The set K_h is nonempty, since h is contained in it. Furthermore, it is clear that K_0 is a convex cone. Since any convergent sequence in $H_0^1(\Omega)$ has an a.e. pointwise convergence subsequence, it also follows that K_0 and thus K_h is closed. \square

Next, we state the ingredients for a variational form of (2.1): For a fixed $a \in L_\infty(\Omega)$ with $a \geq c_0 > 0$, let the bilinear form b and the linear form l be defined by

$$b_a(u, v) := \int_{\Omega} a(x) \nabla u(x) \cdot \nabla v(x) dx, \quad \text{and} \quad l(v) := \int_{\Omega} f(x) v(x) dx. \quad (2.3)$$

With this, we can write (2.1) as the convex unconstrained optimization problem

$$u = \arg \min_{v \in H_0^1(\Omega)} J_a(v), \quad \text{with} \quad J_a(v) := \frac{1}{2} b_a(v, v) - l(v) + i_{K_h}(v), \quad (2.4)$$

where i_{K_h} denotes the indicator function

$$i_{K_h}(v) = \begin{cases} 0, & v \in K_h, \\ \infty, & \text{else.} \end{cases}$$

Note that $i_{K_h}(v)$ is a convex functional, and its subgradient is the normal cone, i.e.,

$$\partial i_{K_h}(v) = N_{K_h}(v) := \{v^* \in H^{-1}(\Omega) \mid \langle v^*, v - u \rangle \leq 0, \quad \forall v \in K_h\},$$

see, e.g., [3, Def. 9.5.2]. For later reference, and given a solution u of (2.1) or (2.4), we also define the contact area K_c , i.e., the set where the constraints are active, as

$$K_c := \{x \in \Omega \mid u(x) = h(x)\}, \quad (2.5)$$

which has to be understood modulo nullsets, analogous to the definition of the essential support. Concerning the solvability of (2.1), we have the following standard results:

Theorem 2.2. *Let $f \in H^{-1}(\Omega)$, $h \in H_0^1(\Omega)$, and $a \in L_\infty(\Omega)$ with $a \geq c_1$. Then, there exists a unique solution $u \in H_0^1(\Omega)$ of (2.1), which is uniquely characterized by the variational inequality*

$$b_a(u, u - v) - l(u - v) \geq 0, \quad \forall v \in H_0^1(\Omega) \cap K_h.$$

Proof. The existence and uniqueness of $u \in H_0^1(\Omega)$ follow by considering the transformation $\tilde{u} = u - h$, and noting that the minimization problem for \tilde{u} is a minimization over a closed convex set K_0 with a bounded and $H_0^1(\Omega)$ -continuous, strictly coercive functional. The coercivity itself follows from standard Poincare-inequality estimates. The optimality condition of this minimization problem can be stated as

$$b_a(u, \cdot) - l(\cdot) + \partial i_{K_h}(u) = b_a(u, \cdot) - l(\cdot) + N_{K_h}(u) \ni 0. \quad (2.6)$$

Considering $v^* := b_a(u, \cdot) - l(\cdot)$ as an element in $H^{-1}(\Omega)$, it follows that $-v^* \in N_{K_h}(u)$, which yields the variational inequality. Conversely, since the problem is convex, the variational inequality yields the first-order optimality condition, which is sufficient. \square

The optimality conditions (2.6) may be written in the form of Lagrange multipliers:

Theorem 2.3. *Under the assumptions of Theorem 2.2, the solution $u \in H_0^1(\Omega)$ of (2.1) is characterized by the following condition: There exists a $\lambda \in H^{-1}(\Omega)$ such that*

$$b_a(u, v) = l(v) + \langle \lambda, v \rangle, \quad \forall v \in H_0^1(\Omega), \quad (2.7)$$

$$u \geq h, \quad \text{a.e. in } \Omega, \quad (2.8)$$

$$\langle \lambda, v - u \rangle \geq 0, \quad \forall v \in K_h. \quad (2.9)$$

Proof. This follows from, e.g., [3, Thm. 9.5.5]. Note that the constraint qualification is satisfied, since the functional $u \mapsto \frac{1}{2}b_a(u, u) - l(u)$ is continuous. \square

Next, following [3, p. 339], we rewrite the above problem into a KKT-type condition. For this, note that we may chose $v = h$ in (2.9) and then $v = 2u - h \in K_h$ to find that $\langle \lambda, u - h \rangle = 0$. Inserting this into (2.9) and setting $v = h + w$, $w \geq 0$, we find that $\langle \lambda, w \rangle \geq 0$ for all $w \geq 0$. This is the weak form of the pointwise constraint $\lambda \geq 0$. Thus, we obtain the equivalent optimality conditions

$$b_a(u, v) = l(v) + \langle \lambda, v \rangle, \quad \forall v \in H_0^1(\Omega), \quad (2.10)$$

$$u \geq h, \quad \text{a.e. in } \Omega, \quad (2.11)$$

$$\langle \lambda, w \rangle \geq 0, \quad \forall w \geq 0, \quad (2.12)$$

$$\langle \lambda, h - u \rangle = 0. \quad (2.13)$$

Conversely, taking $v = h + w$, it follows that these conditions imply (2.7)–(2.9), and thus they are equivalent. Furthermore, under the assumption(!) that λ is more regular than $H^{-1}(\Omega)$ and that it can be represented by an $L_2(\Omega)$ -function, such that $\langle \lambda, v \rangle = \int \lambda(x)v(x) dx$ and if u, a, f are also sufficiently regular to be able to write (2.10) in its strong form, then the above conditions yield the classic KKT system

$$\begin{aligned} -\operatorname{div}(a\nabla u) &= f + \lambda, & \text{in } \Omega, \\ u &= 0, & \text{a.e. on } \partial\Omega, \\ \lambda &\geq 0, & \text{a.e. in } \Omega, \\ u &\geq h, & \text{a.e. in } \Omega, \\ \lambda(u - h) &= 0, & \text{a.e. in } \Omega, \end{aligned}$$

which one can understand as the “completion” of (1.1) required for well-definedness.

Instead of a KKT system, the optimality condition (2.6) may also be rewritten in a fixed-point form. For this, consider the projector onto the optimality constraint space:

$$P_{K_h} y := \arg \min_{v \in K_h} \frac{1}{2} \|v - y\|_{H_0^1(\Omega)}^2 = \arg \min_{v \in H_0^1(\Omega)} \frac{1}{2} \|v - y\|_{H_0^1(\Omega)}^2 + i_{K_h}(v), \quad \forall y \in H_0^1(\Omega).$$

The minimizer above exists due to standard arguments [7], and is characterized by

$$P_{K_h} y = (I + \partial i_{K_h})^{-1} y, \quad (2.14)$$

which is single valued. Note that if $y \in H^{-1}(\Omega)$, then $P_{K_h} y$ can still be well-defined by adapting the above minimization problem, and replacing I in (2.14) with the embedding

$$\iota : H_0^1(\Omega) \rightarrow H^{-1}(\Omega), \quad y \mapsto \left(v \mapsto \langle y, v \rangle_{H_0^1(\Omega)} \right).$$

With this, we can rewrite (2.6) in a fixed-point form, namely

$$\begin{aligned} uu + \tau (b_a(u, \cdot) - l(\cdot)) + \tau \partial i_{K_h}(u) &\ni uu \\ \iff uu + \tau \partial i_{K_h}(u) &\ni uu - \tau (b_a(u, \cdot) - l(\cdot)) \\ \iff u &= P_{K_h}(uu - \tau (b_a(u, \cdot) - l(\cdot))), \end{aligned}$$

for an arbitrary $\tau > 0$, and where we note that $\tau \partial i_{K_h}(u) = \partial i_{K_h}(u)$. Applying a fixed-point iteration now yields the proximal gradient method (see, e.g., [8])

$$u_{n+1} = P_{K_h}(uu_n - \tau (b_a(u_n, \cdot) - l(\cdot))), \quad (2.15)$$

which can be used to solve the forward problem. The drawback of this formulation is the need of the $H_0^1(\Omega)$ -projection instead of the convenient $L_2(\Omega)$ -projection, given by

$$P_{K_h}^{L_2} y = h + \max(y - h, 0).$$

However, this drawback can be remedied in a finite-dimensional context; cf. Section 5.

Boundary constraints: Note that instead of inner constraints caused by an indenter, one can also consider an analogous setting to (1.1) or (2.1) with boundary constraints. For example, assume that we are given a contact area $\Gamma_c \subset \partial\Omega$ on which we have the constraint $u(x) \geq h(x)$, and let, for simplicity, $u = 0$ on $\Gamma_0 := \Omega \setminus \overline{\Gamma_c}$. Furthermore, let

$$H_{0,\Gamma_0}^1(\Omega) := \{v \in H^1(\Omega) \mid v = 0 \text{ on } \Gamma_0\},$$

and, given $h \in H_{0,\Gamma_0}^1(\Omega)$, define the modified constraint set as

$$K_h^{\text{bnd}} := \{v \in H^1(\Omega) \mid v(x) \geq h(x) \text{ a.e. in } \Gamma_c\}.$$

Analogously to (2.4), we then consider the following contact problem in functional form:

$$u = \arg \min_{v \in H_{0,\Gamma_0}^1(\Omega)} J_a^{\text{bnd}}(v), \quad \text{with} \quad J_a^{\text{bnd}}(v) := \frac{1}{2} b_a(v, v) - l(v) + i_{K_h^{\text{bnd}}}(v). \quad (2.16)$$

By continuity of the trace operator, the set K_h^{bnd} is again a closed convex affine cone. Hence, all of the above characterizations for the inner constraint problem (2.1) or (2.4) also hold in a similar form for (2.16) with a Lagrange multiplier in $H^{-1/2}(\Gamma_c)$, which now has the interpretation of an additional Neumann boundary condition on Γ_c .

3 The inverse contact problem

In this section, we consider the inverse contact problem of finding the coefficient a from either a single or multiple (direct or indirect) measurements of u . We define

The inverse contact problem: Given $f_i \in H^{-1}(\Omega)$ and $h_i \in H_0^1(\Omega)$ for $i = 1, \dots, K$, as well as observation operators $B_i : H^1(\Omega) \rightarrow L_2(\Omega'_i)$, with $\Omega'_i \subseteq \Omega$, find the coefficient a from data

$$y = (B_i u_i)_{i=1}^K,$$

where u_i is a solution of (2.1) with coefficient a and given forces f_i and constraints h_i .

In case that the observation operator B is the identity and $\Omega'_i = \Omega$, we have full (internal) measurements of u_i on Ω . Next, we define the parameter-to-data map

$$\begin{aligned} F : D(F) \subset X &\rightarrow \prod_{i=1}^K L_2(\Omega'_i), \\ a &\rightarrow (B_i u_i)_{i=1}^K, \end{aligned} \tag{3.1}$$

for some $X \subseteq L_\infty(\Omega)$, where

$$D(F) := \{a \in X \mid c_1 \leq a(x) \leq c_2 \text{ a.e. in } \Omega\}.$$

With this, the inverse contact problem can be written in the standard form

$$F(a) = y, \tag{3.2}$$

which is a generalization of the well-known coefficient inverse problem of finding the coefficient a in the equation $-\operatorname{div}(a\nabla u) = f$ from full or partial knowledge of u . This classic coefficient inverse problem and the inverse contact problem are related as follows:

- If the Lagrange multiplier λ were known in all instances, then the contact problem could be treated without any constraints by just considering the PDE, thus reducing to the classical problem. However, λ is unknown, cannot be measured, and depends implicitly on the unknown a , making the contact problem more difficult.
- If the contact area K_c defined in (2.5) is known (and sufficiently regular), then the (inverse) contact problem reduces to a boundary value problem in $\Omega \setminus K_c$, where u takes the Dirichlet boundary condition h at ∂K_c . In this case, we are again facing a standard coefficient problem in $\Omega \setminus K_c$. However, in this paper, we are reluctant to assume the knowledge of K_c , since this is only possible when considering full measurements of u (which may additionally be contaminated by noise). Since in some elastic indentation tests the indenter geometry may obstruct access to u near the contact area, measurements cannot be reliably obtained in its immediate vicinity in these cases. Hence, we here consider a general case where observations are potentially only available away from the contact area.

Another key difference between the classic coefficient inverse problem and the inverse contact problem are non-uniqueness issues for the reconstruction of a that arise due to the constraints, which we investigate in the subsequent section.

3.1 Uniqueness and non-uniqueness for the constrained and unconstrained inverse problems

First, we recall some known standard uniqueness and non-uniqueness results for the unconstrained (i.e., without the constraint $u \geq h$) coefficient inverse problem: Uniqueness of a given full measurements of u was shown in [58] (see also [52]) if the (Richter) condition $\max\{|\nabla u|, \Delta u\} > c_1 > 0$ holds in Ω and if a is known on a relevant part of the boundary. Furthermore, in [1] uniqueness was established for the Dirichlet problem in two dimensions if the coefficient a is known on the boundary and the Dirichlet data have a finite number of maxima and minima. Finally, the authors of [14] have shown uniqueness for the homogeneous problem on a set of characteristic lines.

In the case of multiple measurements, [6] has established uniqueness (up to a multiplicative constant) for the homogeneous problem and in case of Dirichlet boundary conditions from full measurements of $\frac{n(n+3)}{2}$ solutions u_i (the anisotropic case was treated in [4]). In the absence of such conditions, the non-uniqueness of the coefficient is clear: As a simple example, take in 2D a solution $u(x, y) = cx + d$, $c, d \in \mathbb{R}$. Then any function depending only on y can be added to the coefficient a without affecting this solution.

The above uniqueness conditions can immediately be transferred also to the constrained problem but only in the non-contact region, where the PDE holds. However, the contact area adds some additional difficulty, since we can show that the coefficient a cannot be recovered at the interior $\text{int}(K_c)$ of the contact area K_c . In particular, we have the following non-uniqueness result:

Theorem 3.1. *Let $a \in C^1(\Omega)$, $f \in C(\Omega)$, $h \in C^2(\bar{\Omega})$, and define*

$$D := \text{int}(\{x \in \text{int}(K_c) \mid \nabla h(x) = 0\}) \cup \{x \in \text{int}(K_c) \mid \text{div}(a\nabla h(x)) \neq f(x)\} .$$

Furthermore, let u_a be a solution of the contact problem (2.1) with given a, f, h . Then, there exists an $\tilde{a}(x) := a(x) + \delta a \in D(F)$, where $\delta a \in C^1(\Omega)$ is supported in a compact subset of D such that u_a is also a solution of (2.1) with the modified coefficient \tilde{a} . In particular, a is not uniquely determined by u_a in any compact subset of D .

Proof. First, consider a coefficient perturbation in the interior of the contact area, i.e., $\tilde{a}(x) := a(x) + \delta a(x)$ for some $\delta a(x)$, with

$$\text{supp}(\delta a) \subset \text{int}(K_c) \quad \text{and} \quad \delta a \in L_\infty(\Omega) \cap C^1(\text{int}(K_c)) ,$$

the precise form of which is specified in detail below. We now show that such a perturbation does not influence the solution u_a . For this, let the bilinear form b_a be given as in (2.3). The optimality conditions for the given solution u_a and the associated Lagrange multiplier λ_a and for \tilde{a} are

$$b_{\tilde{a}}(u, v) = b_a(u, v) + b_{\delta a}(u, v) = l(v) + \langle \lambda_a v \rangle + b_{\delta a}(u, v) ,$$

in addition to the conditions (2.11)–(2.13). Since δa has support in K_c , we have $b_{\delta a}(u, v) = b_{\delta a}(h, v)$. Next, define the Lagrange multiplier

$$\tilde{\lambda} := \lambda_a + b_{\delta a}(h, \cdot) ,$$

which represents an element in $H^{-1}(\Omega)$. With this $\tilde{\lambda}$, the first condition, (2.10), holds. Condition (2.13) holds since $u = h$ at the support of δa , and thus $b_{\delta a}(h, u - h) = 0$.

Hence, we now only have to verify (2.12). For this, note first that due to the smoothness assumptions, the set of all x in $\text{int}(K)$ with $\text{div}(a\nabla h(x)) \neq f(x)$ is open, and thus D is open. Furthermore, again due to the smoothness assumptions, we have

$$\lambda_a = -\text{div}(a\nabla u) - f = -\text{div}(a\nabla h) - f, \quad \text{in } \text{int}(K), \text{ pointwise in } D,$$

as well as $\tilde{\lambda} = \lambda_a - \text{div}(\delta a \nabla h)$. If $x \in \text{int}(\{x \in \text{int}(K_c) \mid \nabla h(x) = 0\})$, it follows that $\tilde{\lambda} = \lambda_a$, and thus positivity of $\tilde{\lambda}$ is inherited from λ_a , establishing (2.12) in this case.

On the other hand, for all $x \in \tilde{D} := \text{int}(\{x \in \text{int}(K_c) \mid \text{div}(a\nabla h(x)) \neq f(x)\})$, we have $\lambda_a \neq 0$ by the pointwise equality, and thus $\lambda_a > 0$ in this set. Hence, for an arbitrary compact subset, we have $\lambda_a(x) \geq c_1 > 0$ by the Heine theorem. Now take an arbitrary $\phi \in C^1(\Omega)$ with compact support in \tilde{D} and set $\delta a := \varepsilon \phi$ with $\varepsilon > 0$. Then

$$\tilde{\lambda} = \lambda_a - \varepsilon \text{div}(\phi \nabla h) \geq c_1 - \varepsilon \|\phi\|_{C^1} \|h\|_{C^2}.$$

By choosing ε small enough, we find $\tilde{\lambda} \geq 0$, verifying (2.12) and completing the proof. \square

The above theorem roughly states that we cannot identify the coefficient a at the contact area. (More precisely, formally this only holds on the contact area where $\nabla h = 0$ or where $\lambda_a \neq 0$. However, the case that this does not agree with K_c represents an exceptional case which corresponds to areas where no force is required to keep contact; thus Theorem 3.1 can be (informally) considered to hold for the full contact area K_c .) Note that at the exceptional set $K_c \setminus D$, one could identify a by using the equation $\text{div}(a\nabla h) = f$ up to boundary conditions of a as in the classical case.

In addition to the non-uniqueness in the contact area above, we can illustrate further examples of non-uniqueness even away from the contact area: this is related to the non-connectedness of the non-contact area and to the lack of the Richter condition (see above) therein. Note that for the homogeneous problem without constraints, the Richter conditions are not too restrictive, since the gradient and the Laplacian cannot vanish on an open set, which allowed the uniqueness result in [1] discussed above. In contrast, this might not be the case for some standard constrained problems:

- (i) The contact problem can induce further non-uniqueness issues even outside of the contact area K_c , e.g., if the contact area is not connected: Assume $f = 0$ and let K_c be an annulus as in Figure 3.1. Then, we have non-uniqueness at the annulus contact area but also *inside* of it, since there $u = \text{const.}$ and thus $\nabla u = \Delta u = 0$.
- (ii) In Figure 3.2, we illustrate another instance of non-uniqueness due to the violation of the Richter condition in a 1D example. Here, $f = 0$ and the solution u , $x \in [0, 1]$, satisfies the equation $-(au')' = \lambda$, with the constraint given by h indicated as the upper boundary of the blue dashed object (indenter). The graph of u is printed as a thick black line for the case when a is a constant: the solution

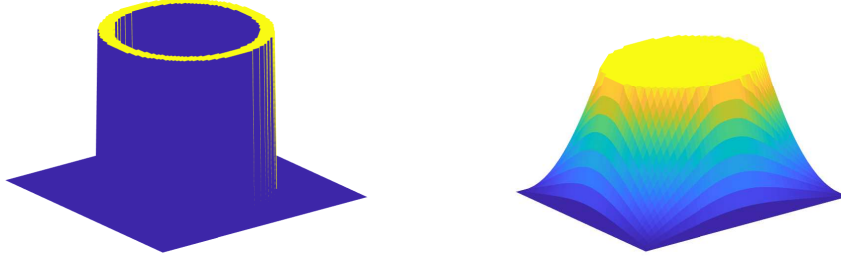


Figure 3.1: Left: constraint function h . Right: solution of $\operatorname{div}(a\nabla u) = 0$. Inside the annulus contact region, the coefficient a is not identifiable.

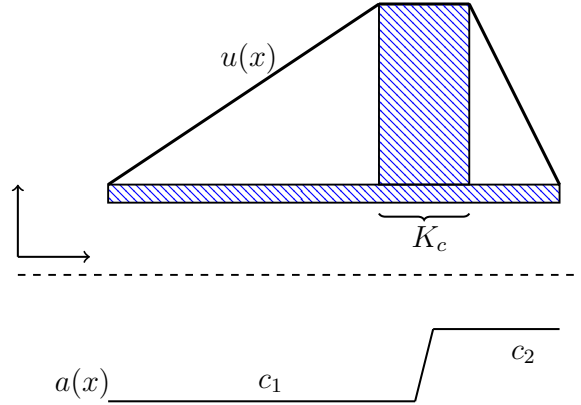


Figure 3.2: Illustration of a non-unique parameter a in a 1D contact problem: The solution is piecewise constant over the constraint given by h (blue dashed object). Below is an illustration of the non-uniqueness of a : It is piecewise constant with smooth connection inside the contact area. The constants $c_1, c_2 > 0$ can be chosen arbitrarily.

is piecewise constant with contact area K_c . The Lagrange multipliers are δ -distribution supported on the boundary of the contact area. However, it turns out that the same solution u is obtained if a is piecewise constant with constants c_1 and c_2 and a smooth connection inside the contact area as indicated in the figure. Thus, non-uniqueness in a is apparent and occurs here due to the non-connectedness of the non-contact area.

Note that this example models a string spanned over a fixed bridge, and intuitively it is clear that changing the stress (i.e., a) or the material uniformly does not alter the shape of the string. Note that a similar example can be found in a 2D setting by extending u constant into y -direction and modifying the boundary conditions in (2.1) to homogeneous Neumann boundary condition at $y = 0$ and $y = 1$.

The last example of non-uniqueness can be generalized to the following theorem:

Theorem 3.2. *Let u satisfy the homogeneous model problem (1.1) (i.e., with $f = 0$ and Dirichlet boundary data g). Furthermore, assume that the non-contact area $\{u \neq h\}$ splits into n disjoint regions Ω_i , $i = 1, \dots, n$. Then, there are n constant c_i such that the coefficient a can be multiplied by c_i on Ω_i giving rise to the same solution u .*

Proof. On each of the regions Ω_i , u solves a Dirichlet problem with Dirichlet data either g or h . Since there, a can be multiplied by a constant without altering the PDE, the result immediately follows. \square

It should be noted that, for instance, in the annulus problem (but also for the problem in Theorem 3.2 as long as the contact area remains the same), the non-uniqueness is not necessarily resolved by multiple measurements: If the contact at the annulus is always active, then inside the annulus, the multiple solutions are always constant and thus linearly dependent. The non-uniqueness problem remains. Thus, to improve identifiability for multiple measurements, one should design the experiments (i.e., by altering f or h) such that the contact area changes (see the last example in Section 6.2).

4 Regularization approaches

In this section, we consider regularization approaches for the inverse contact problem. Since its formulation given in (3.2) is in standard form, we can use standard methods [20] such as Tikhonov regularization, which computes an approximate solution as

$$a_\alpha := \arg \min_{a \in D(F)} \|F(a) - y\|^2 + \alpha \|a\|_X^2, \quad (4.1)$$

with α a regularization parameter (see, e.g., [20]). There exist many variations on this approach: the penalty term $\|a\|_X^2$ may be replaced by general Banach space penalties (e.g., [36]) or the data-fit term by more general expressions (e.g., [61]). Furthermore, for the non-constrained problem, it became popular to weakly include the PDE into the functional as in the all-at-once approach [44–46]. By tailoring the data-fit term, one can establish the energy-functional variational formulation leading to convex optimization problems; for the unconstrained problem, this has been put into an abstract framework in [28, 29]; for the constrained problem – more precisely for the variational inequality case and for *full* observations – this has been extended in [30–33, 42, 49]. Note that, since we here treat the limited data case, these latter approaches cannot be straightforwardly extended to our case. Hence, the most flexible choice here is standard Tikhonov regularization and related iterative regularization schemes such as variants of gradient descent for the least-squares functional with appropriate stopping rules.

In order to verify the standard assumptions required for the convergence analysis of Tikhonov regularization, we first need to analyze of the parameter-to-solution mapping:

Theorem 4.1. *Let $f_i \in H^{-1}(\Omega)$, $h_i \in H_0^1(\Omega)$, $i = 1, \dots, n$, and F be defined as in (3.1), where X is a Hilbert space compactly embedded into $L_\infty(\Omega)$. Assume that B_i is continuous from the weak $H^1(\Omega)$ topology into $L_2(\Omega_i)$. Then F is weakly sequentially closed.*

Proof. Without loss of generality, we can assume that $n = 1$, and thus write f, h, u, B instead of f_i, h_i, u_i, B_i throughout this proof. Now for any $a \in D(F)$, let $u_a \in H_0^1(\Omega)$ be the well-defined minimizer of J_a defined in (2.4). Assume that $a_n \rightarrow_X a$ and $F(a_n) \rightarrow z$. Then $a \in D(F)$, and with the Poincare inequality, it follows that

$$c_1 \|u_{a_n}\|_{H^1}^2 \leq \int_{\Omega} a_n(x) |\nabla u_{a_n}(x)|^2 dx \leq \int_{\Omega} a(x) |\nabla u_{a_n}(x)|^2 dx + i_{K_h}(u_{a_n}) \leq c_2 \int_{\Omega} |\nabla h| dx.$$

Hence, u_{a_n} is uniformly bounded in $H^1(\Omega)$ and has a weakly convergent subsequence

$$u_{a_n} \rightharpoonup_{H^1} w.$$

It is not difficult to show that J_a is lower semicontinuous in $H^1(\Omega)$: This is obvious for the first part ($\frac{1}{2}b_a(v, v) - l(v)$), and the lower semicontinuity of $i_{K_h}(u)$ with respect to the norm convergence in $H^1(\Omega)$ follows from the fact that K_h is closed in $H^1(\Omega)$; see Lemma 2.1. Since J_a is also convex, it is weakly lower semicontinuous. Furthermore,

$$\begin{aligned} J_a(u_{a_n}) &= \int_{\Omega} a(x) |\nabla u_{a_n}(x)|^2 dx - \int_{\Omega} f(x) u_{a_n}(x) dx + i_{K_h}(u_{a_n}) \\ &= \int_{\Omega} a(x) |\nabla u_{a_n}(x)|^2 dx - \int_{\Omega} f(x) u_{a_n}(x) dx \\ &= \int_{\Omega} a_n(x) |\nabla u_{a_n}(x)|^2 dx - \int_{\Omega} f(x) u_{a_n}(x) dx \\ &\quad + \int_{\Omega} (a(x) - a_n(x)) |\nabla u_{a_n}(x)|^2 dx \\ &\leq J_{a_n}(v) + \int_{\Omega} (a(x) - a_n(x)) |\nabla u_{a_n}(x)|^2 dx \\ &\leq J_a(v) + \int_{\Omega} (a(x) - a_n(x)) |\nabla v(x)|^2 dx + \int_{\Omega} (a_n(x) - a(x)) |\nabla u_{a_n}(x)|^2 dx, \end{aligned}$$

for any $v \in H_0^1(\Omega)$ due to the minimality property of u_{a_n} . Now since due to the compact embedding of X in $L_{\infty}(\Omega)$ there holds $\|a_n - a\|_{\infty} \rightarrow 0$, it follows that

$$\int_{\Omega} (a(x) - a_n(x)) |\nabla u_{a_n}(x)|^2 dx \leq \|a_n - a\|_{\infty} \int_{\Omega} |\nabla u_{a_n}(x)|^2 dx \leq C \|a_n - a\|_{\infty} \rightarrow_{n \rightarrow \infty} 0. \quad (4.2)$$

Similarly, we obtain

$$\int_{\Omega} (a(x) - a_n(x)) |\nabla v(x)|^2 dx \rightarrow_{n \rightarrow \infty} 0.$$

Combining the above, we find that for all $v \in H_0^1(\Omega) \cap K_h$ there holds

$$J_a(w) \leq \liminf_n J_a(u_{a_n}(x)) \leq J_a(v).$$

Hence, w is a minimizer and thus by uniqueness, we obtain $w = u_a$. \square

Due to the above theorem, the classic convergence analysis of Tikhonov regularization is applicable, which yields the usual convergence results [20, 21]. However, it does not tell us how to calculate the regularized solution a_α , i.e., how to minimize (4.1). In addition, we expect (but do not have a proof) that the parameter-to-solution map F is non-differentiable in this case, which would imply that standard gradient descent or iterative regularization methods cannot be applied to our model problem. Recall that the simplest iterative method, namely Landweber iteration (e.g. [20, 47, 48]), defined by

$$a_{k+1} = a_k - \tau F'(a_k)^*(F(a_k) - y^\delta) \quad (4.3)$$

requires Fréchet-differentiability of the forward operator. The same holds for other schemes such as (iteratively regularized) Gauss-Newton methods as well as Levenberg-Marquard-type methods [47]. Since we strongly doubt that the Fréchet derivative exists in our case, such approaches are not available to us without substantial modifications.

To support the potential (and conjectured) non-differentiability of our forward operator F , we note that for some related problems in control theory, for instance, for the mapping $f \rightarrow u$ in the constrained case, generalized differentiability results (e.g., semismoothness) have been established in [15, 16, 57]. In particular, [57, Theorem 5.6] indicates that in this case the generalized derivatives are typically multi-valued, which implies that classical differentiability cannot hold. Since the linearization of the parameter-to-solution map leads to exactly such mappings (with $-\operatorname{div}(h\nabla u)$ as the right-hand side), this should serve as a convincing argument that our inverse problem is also not classically differentiable. Verifying, e.g., semismoothness for F in appropriate spaces would be a non-trivial investigation far outside the scope of the present paper.

Note that iterative regularization schemes with generalized derivatives (e.g. Bouligand derivatives) have been developed for inverse problems [17, 18, 43], but since we are unsure if our problem allows for such derivatives (in the required spaces!) we do not make use of them here. Potentially, the SCD semismooth* Newton method could be used for minimizing (4.1), since it only requires weak differentiability conditions [23–26].

In the following, we introduce our proposed iterative regularization method for solving the inverse model problem, which essentially consist of a variant of Landweber iteration (4.3) with a modified derivative in place of $F'(a_k)$. Additionally, we use Nesterov acceleration to speed up the reconstruction process [55]. Our reasoning for this choice is as follows: Of course, for a fast iteration, one could try to use second order methods (such as Gauss-Newton, IRGN, Levenberg-Marquard, etc.) as mentioned above. However, two reasons speak against it: Firstly, these methods – in their exact form – require the solution of a large linear system involving the Fréchet-derivative of the forward operator, which we would like to avoid for reasons of efficiency and simplicity. (One could, of course, use inexact Newton methods such as [59], but this adds another level of approximation schemes which we would like to avoid). Secondly, since in our proposed approach we anyways replace the Fréchet-derivative by an approximation, we expect that second-order methods are more sensitive to taking this wrong derivative. (Partly, this can be seen from the fact that the convergence theory of several of these methods rely on range-invariance rather than the tangential cone-type conditions [47].)

Thus, we propose to use a Nesterov-accelerated Landweber method for solving the inverse model problem (3.2), which we found to be a robust and efficient regularization scheme. We describe this method in detail in the following section and, to avoid substantial technical difficulties, only in a finite-dimensional (discretized) setup.

5 The finite-dimensional problems

In this section, we consider the forward and inverse contact problems in a discretized setting, and discuss different (iterative) methods for the efficient solution of the direct problem, namely a projected gradient method with its accelerated variant and a barrier method. Although other methods are certainly possible, the rationale for this choice is their simplicity and, as we shall see, their integrability into the regularization schemes.

5.1 The discretized forward contact problem

In order to discretize the forward contact problem, we consider a continuous, piecewise linear finite-element nodal basis over a (uniform) triangulation of the domain Ω , i.e.,

$$u = \sum_{i=1}^N u_i \phi_i, \quad f = \sum_{i=1}^N f_i \phi_i, \quad \text{and} \quad h := \sum_{i=1}^N h_i \phi_i.$$

The minimization problem (2.1) is then considered over the corresponding finite element space, and the constraint $u \geq h$ is replaced by nodal constraints on the FEM nodes, i.e.,

$$u_i \geq h_i, \quad \forall i = 1, \dots, N.$$

The resulting minimization problem can again be rewritten as in the continuous setting. In this case, the Lagrange multiplier λ then corresponds to a vector $\boldsymbol{\lambda} = (\lambda_i)_{i=1}^N$, and the KKT conditions are given in the usual form: Let A denote the stiffness matrix, \mathbf{f} the load vector, and \mathbf{u}, \mathbf{h} the coefficient vectors of the corresponding basis functions. Then the KKT system of the discretized contact problem has the form: Find $\mathbf{u}, \boldsymbol{\lambda}$ with

$$A\mathbf{u} = \mathbf{f} + \boldsymbol{\lambda}, \tag{5.1}$$

$$u_i \geq h_i, \quad \forall i = 1, \dots, N, \tag{5.2}$$

$$\lambda_i \geq 0, \quad \forall i = 1, \dots, N, \tag{5.3}$$

$$\lambda_i(u_i - h_i) = 0, \quad \forall i = 1, \dots, N. \tag{5.4}$$

In order to solve this forward contact problem in the discretized setting, we consider two approaches, an accelerated projected gradient method and a barrier method:

(Accelerated) projected gradient method. For the projected gradient method, we first consider the proximal gradient method (2.15) on the discrete level, i.e.,

$$\mathbf{u}_n = P_{K_h}(\mathbf{u}_n - \tau(A\mathbf{u}_n - \mathbf{f})), \tag{5.5}$$

where P_{K_h} now denotes the projector onto $u_i \geq h_i$, which on the coefficient level reads

$$(P_{K_h} \mathbf{y})_i = h_i + \max \{y_i - h_i, 0\}, \quad \text{for } \mathbf{y} = (y_i)_{i=1}^N.$$

To speed up the iteration, we use Nesterov acceleration [55], which in this case yields

$$\begin{aligned} \mathbf{u}_n &= P_{K_h}(\mathbf{z}_n - \tau(A\mathbf{z}_n - \mathbf{f})), \\ \mathbf{z}_n &= \mathbf{u}_n + \frac{t_{n-1} - 1}{t_n}(\mathbf{u}_n - \mathbf{u}_{n-1}), \end{aligned} \quad (5.6)$$

where $t_{n+1} := \frac{1}{2}(1 + \sqrt{1 + 4t_n^2})$ and τ is a stepsize parameter which has to be chosen smaller than $\|A\|$. This method works well for the test problems presented in Section 6.

Barrier method. As an alternative to the projected gradient method, we also consider a barrier method for solving the discretized constrained optimization problem. The reason for a second method is that the mapping $a \rightarrow \mathbf{u}$ is presumably not continuously differentiable with respect to the parameter a , as can be seen from the max-function appearing in the projected gradient method (5.5), and by our remarks on semismoothness above. With regards to the inverse problem, for which differentiability is strongly beneficial, we therefore consider a smooth approximation of the constrained forward problem using a log-barrier function. For this, we define a barrier function (for the constraint $u_i \geq h_i$) as follows:

$$g(\mathbf{u}) := \begin{cases} -\log(u_i - h_i + \theta), & u_i \geq h_i, \\ \infty, & \text{else,} \end{cases}$$

where $\theta > 0$ is a safeguard parameter ensuring a finite value of the logarithm. The approximate solution of the constrained forward problem is then found by minimizing

$$J_b(\mathbf{u}) = \frac{1}{2} \mathbf{u}^T A \mathbf{u} - \mathbf{f}^T \mathbf{u} + \mu g(\mathbf{u}), \quad \text{s.t. } u_i \geq h_i, \quad \forall i = 1, \dots, N, \quad (5.7)$$

where μ denotes a penalty parameter which is updated during the iteration, and A is the stiffness matrix including the given homogeneous Dirichlet boundary conditions. In order to solve this minimization problem, we use the projected Newton-type method

$$\mathbf{u}_{n+1} = P_{K_h}(\mathbf{u}_n - \tau \nabla^2 J_b(\mathbf{u}_n)^{-1} \nabla J(\mathbf{u}_n)), \quad (5.8)$$

with a fixed stepsize τ and an iteratively updated μ and θ , which are chosen as

$$\mu_{n+1} = 0.9 \cdot \mu_n, \quad \text{and} \quad \theta_{n+1} = \max \{0.9 \cdot \theta_n, 10^{-12}\}.$$

Note that the constraint $u_i \geq h_i$ in (5.7) ensures that $g(\mathbf{u})$ is smooth on the admissible set (of \mathbf{u}), and consequently $J_b(\mathbf{u})$ is (twice) differentiable and thus (5.8) is well-defined.

5.2 The discretized inverse contact problem

To solve the discretized inverse contact problem, we consider regularization schemes as discussed in Section 4. Since the forward operator F is nonlinear, iterative optimization methods are typically used to minimize the corresponding Tikhonov functional (4.1). However, most of these methods require F to be differentiable with respect to a , which is not necessarily the case for the contact problem. Hence, for solving the inverse problem, we slightly modify the forward problem by considering the differentiable barrier problem formulation (5.7) instead. In a sense, we approximate the forward operator F by a differentiable operator \tilde{F} , for which we then use standard Tikhonov regularization. This approximation can be justified by noting that regularization theory allows for small perturbations of the operator F without impairing the convergence analysis.

Hence, in place of the true forward operator F , we consider the approximate mapping $\tilde{F}a := B\tilde{\mathbf{u}}$, where $\tilde{\mathbf{u}}$ denotes the solution (minimizer) of the barrier problem (5.7) in the discretized FEM setting. It is not difficult to verify that $\tilde{\mathbf{u}} = \tilde{\mathbf{u}}(a)$ satisfies

$$A\tilde{\mathbf{u}} - \mathbf{f} + \mu \frac{1}{\tilde{\mathbf{u}} - \mathbf{h} + \theta} = 0.$$

Here and below, the vector $\frac{1}{\tilde{\mathbf{u}} - \mathbf{h} + \theta}$ stands for the vector $(\frac{1}{\tilde{u}_i - h_i + \theta})_{i=1}^n$, i.e., where the inverse is taken component-wise. Furthermore, with a slight abuse of notation, we also denote by $\frac{1}{\tilde{\mathbf{u}} - \mathbf{h} + \theta}$ and similar expressions the diagonal matrix with entries $(\frac{1}{\tilde{u}_i - h_i + \theta})_i$, $i = 1, \dots, n$, representing the discrete version of the multiplication operator

$$v(x) \rightarrow \left(\frac{1}{\tilde{\mathbf{u}}(x) - \mathbf{h}(x) + \theta} \right) v(x).$$

Next, note that the parameter a only appears inside the stiffness matrix $A = A(a)$, and only as a linear factor. Hence, using the above notation, the Fréchet derivative $\tilde{\mathbf{u}}'(a)b$ can be calculated as the (unique) solution $\tilde{\mathbf{u}}_a$ of

$$A(a)\tilde{\mathbf{u}}_a + A(b)\tilde{\mathbf{u}} + \mu \frac{1}{(\tilde{\mathbf{u}} - \mathbf{h} + \theta)^2} \tilde{\mathbf{u}}_a = 0,$$

and thus

$$\tilde{\mathbf{u}}'(a)b = \left(A(a) + \mu \frac{1}{(\tilde{\mathbf{u}} - \mathbf{h} + \theta)^2} \right)^{-1} A(b)\tilde{\mathbf{u}}.$$

Furthermore, its L_2 -adjoint is given by

$$\tilde{\mathbf{u}}'(a)^* \mathbf{v} = \left(\sum_{n=1}^N \langle \nabla \phi_k, \nabla \phi_n \rangle (\tilde{\mathbf{u}})_k (\mathbf{w})_n \right)_{k=1}^N \approx \nabla \tilde{\mathbf{u}} \cdot \nabla \mathbf{w},$$

where

$$\mathbf{w} := \left(A(a) + \mu \frac{1}{(\tilde{\mathbf{u}} - \mathbf{h} + \theta)^2} \right)^{-1} \mathbf{v},$$

for the derivation of which we used that $(A(a) + \mu \frac{1}{(\tilde{\mathbf{u}} - \mathbf{h} + \theta)^2})$ is a selfadjoint matrix.

The Fréchet derivative $\tilde{F}'(a)$ of the full forward operator \tilde{F} (barrier formulation) including the observation operators (now matrices) B is then simply given by

$$\tilde{F}'(a)b = B \tilde{\mathbf{u}}'(a)b,$$

and the L_2 -adjoint $\tilde{F}'(a)^*$ now reads

$$\tilde{F}'(a)^*y = \tilde{\mathbf{u}}'(a)^*(B^*y).$$

The iterative regularization scheme Having derived all the necessary ingredients above, we can now consider Landweber iteration as our iterative regularization method, which approximates the ground truth coefficient a^\dagger iteratively via (τ is a stepsize)

$$a_{k+1} = a_k - \tau \tilde{F}'(a_k)^*(F(a_k) - y). \quad (5.9)$$

Note that different Hilbert space regularization can be introduced by considering the adjoint $\tilde{F}'(a_k)^*$ between appropriate spaces [40]. Furthermore, in order to accelerate the Landweber iteration (5.9), we propose to use its Nesterov accelerated version [39]:

$$\begin{aligned} b_n &= a_n + \frac{n-1}{n+2}(a_n - a_{n-1}), \\ a_{n+1} &= a_n - \tau \tilde{F}'(b_n)^*(F(b_n) - y). \end{aligned} \quad (5.10)$$

This is the method which was implemented for obtaining our numerical results below.

Note that both methods, (5.9) and (5.10), can be related to Tikhonov regularization by replacing the above least-squares gradient by the gradient of the Tikhonov functional. The results are comparable; the methodical difference is that the iterative schemes have to be terminated by a stopping criteria, e.g., the discrepancy principle, while for the Tikhonov-gradient variant, the regularization parameter has to be selected by a suitable parameter choice rule, and the iteration converges (if certain conditions are satisfied) to a stationary point of the Tikhonov functional.

Concerning the convergence properties of the proposed methods (5.9) or (5.10), we here only sketch how a convergence analysis may be conducted: the main difference of (5.9) and (5.10) to established methods is the use of a “wrong” derivative and its adjoint. However, such a possibility already exists in the seminal article on Landweber iteration for nonlinear inverse problems [34]. There, the main condition which needs to be verified for a successful analysis of (5.9) is the tangential cone-type condition

$$\left\| F(a) - F(\tilde{a}) - \tilde{F}'(\tilde{a})(a - \tilde{a}) \right\| \leq \eta \|F(a) - F(\tilde{a})\|, \quad \eta < \frac{1}{2}.$$

We leave an analysis of this condition for the contact problem to future research.

6 Numerical experiments

In this section, we present a number of numerical experiments illustrating the solution of the forward and inverse contact problem with the methods introduced above. For all

experiments, we use a standard (P_1 -elements) finite-element discretization on a uniform grid over the unit square $[0, 1]^2$ with n gridpoints in each axial direction. The coefficient a was also discretized by P_1 -finite elements, and so was the indenter function h . All of the experiments were conducted in Matlab on a standard desktop computer.

6.1 Forward problem verification

In our first series of tests, we verify the three algorithms for the forward contact problem described above, i.e., the projected gradient method (PG), the Nesterov-accelerated projected gradient method (NPG), and the barrier method (BM). In particular, we investigate how well and how fast these algorithms can approximate an exact solution.

As an error indicator, we use both the maximum-norm and the (discrete) ℓ_2 norms between the computed solution u_{comp} and an exact solution u_{ex} , i.e.,

$$\text{err}_\infty := \|u_{\text{comp}} - u_{\text{ex}}\|_\infty, \quad \text{and} \quad \text{err}_2 := \|u_{\text{comp}} - u_{\text{ex}}\|_{\ell_2}.$$

Here, u_{comp} denotes the solution obtained by one of the above algorithms, while the reference “exact” solution u_{ex} is computed on a refined grid ($n = 500$). Furthermore, as an optimality indicator, we use the residual norm of the KKT system, i.e.,

$$\text{err}_{\text{KKT}} := \left\| \begin{pmatrix} \min(Au - f, 0) \\ \min(u - h, 0) \\ \|(Au - f)(u - h)\|_\infty \end{pmatrix} \right\|_{\ell_2}.$$

Here, the first expression in the norm measures the violation of $\lambda \geq 0$, the second one that of $u \geq h$, and the last one the violation of the KKT conditions. These expressions are computed nodalwise, and the Euclidean norm of all expressions is used above.

For our first test (TestCase 1), we consider the Laplace equation, i.e., $a = 1$ and $f = 0$, with an indenter which is the indicator function on the square $[0.35, 0.65]^2$. The iteration is terminated as soon as err_{KKT} falls below 10^{-8} or a maximum number of iteration (5000) is reached. The only sensitive parameter for our gradient methods is the stepsize τ , which should be chosen such that $\tau \|A\| < 1$; here we use the more conservative choice $\tau = 0.1 / \|A\|$. For the barrier method, we use the stepsize $\tau = 0.1$.

The results of this case are summarized in Table 6.1 and Figure 6.1. In Table 6.1, we summarize various performance indicators (errors and wall-clock CPU-time in seconds), while Figure 6.1 depicts the error curve for the maximum norm (err_∞) and the KKT residual (err_{KKT}) over the number of iterations. From these results, we first observe the relative slowness of the projected gradient method, which as expected is outperformed by the other two methods. The barrier method, being a second-order method, requires the least number of iterations, exhibiting a steep decrease of the KKT residual during the iteration. Furthermore, we see that the NPG method outperforms the PG method: the error is quite small and the solution acceptable even after a moderate (< 1000) number of iterations, after which the error remains almost constant; the method does not terminate because the KKT residual is decreasing slower than for the barrier method.

For our second test (TestCase 2), we perform the same experiment as above but with a different set of parameters. More precisely, for the indenter h we take the indicator

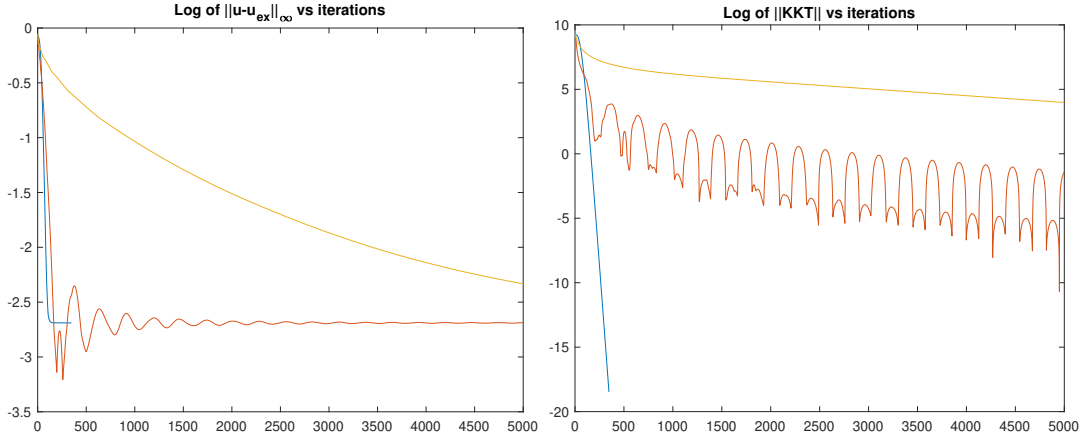


Figure 6.1: Log of err_∞ (left) and log of err_{KKT} (right) vs. the number of iterations for TestCase 1 and a discretization of $n = 40$, for the barrier method (blue), Nesterov-accelerated projected gradient method (red), and projected gradient method (yellow).

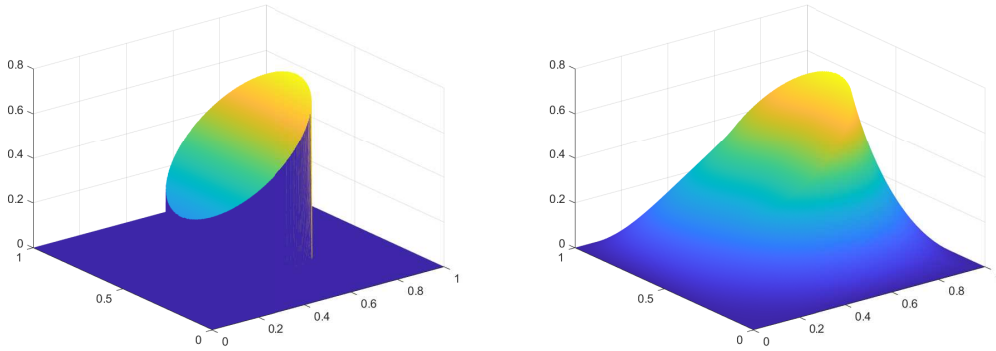


Figure 6.2: Indenter h (left) and solution (right) for TestCase 2.

function of a circle with center $(0.5, 0.5)$ and radius 0.25 , and “cut off” its top by the linear function $g(x_1, x_2) = x_1$; see Figure 6.2(left). Furthermore, we choose

$$\begin{aligned} f(x_1, x_2) &= (-10) \sin(\pi x_1) \sin(2\pi x_2), \\ a(x_1, x_2) &= 1 + \frac{1}{2} \exp(-20((x_1 - 0.4)^2 + (x_2 - 0.5)^2)) \sin(2\pi x_1), \end{aligned}$$

Both the indenter and the corresponding solution are illustrated in Figure 6.2. The results are quite similar to the first experiment; the characteristics are given in Table 6.1.

6.2 Numerical results for the inverse problem

In our second series of tests, we consider the solution of the inverse contact problem via the iterative regularization procedure (5.10) and illustrate some of its features.

Experiment 1. In our first experiment, we consider the identification of the coefficient a from full measurements of u with different indenters and noise levels. As before, we

Table 6.1: Error indicators for various discretizations, methods, and TestCase 1 and 2.

	$\log(\text{err}_\infty)$	$\log(\text{err}_{L_2})$	# iter. for $\text{err}_{\text{KKT}} < 10^{-8}$	CPU-time(s)
TestCase 1				
$n = 20$				
BM	-2.35	-3.2988	323	0.13
NPG	-2.35	-3.2988	3692	1.03
PG	-2.35	-3.2988	4834	0.69
$n = 40$				
BM	-2.6893	-3.6913	347	0.37
NPG	-2.6873	-3.6885	≥ 5000	1.40
PG	-2.3328	-3.1552	≥ 5000	0.80
$n = 80$				
BM	-2.8549	-3.9528	347	1.72
NPG	-2.8875	-4.0151	≥ 5000	1.84
PG	-0.7442	-1.4140	≥ 5000	1.26
$n = 160$				
BM	-2.9466	-4.0876	394	7.00
NPG	-3.3405	-4.2873	≥ 5000	3.51
PG	-0.2463	-1.0694	≥ 5000	2.96
TestCase 2				
$n = 20$				
BM	-2.3029	-4.2973	324	0.12
NPG	-2.3029	-4.2973	3667	0.63
PG	-2.3029	-4.2973	4645	0.45
$n = 40$				
BM	-2.8150	-4.5637	348	0.36
NPG	-2.8150	-4.5637	≥ 5000	0.95
PG	-2.8150	-4.5637	≥ 5000	0.58
$n = 80$				
BM	-3.2752	-5.2024	372	1.74
NPG	-3.2752	-5.1872	≥ 5000	1.45
PG	-1.2072	-2.1834	≥ 5000	1.03
$n = 160$				
BM	-3.9207	-6.1688	395	7.40
NPG	-3.9047	-5.2068	≥ 5000	3.19
PG	-0.6389	-1.7066	≥ 5000	2.74

use a fixed grid on the unit square, now with $n = 50$ nodes in each direction. For the right-hand side, we select $f = 0$, and for the ground truth parameter a^\dagger , we choose

$$a^\dagger(x_1, x_2) := 1 + \frac{1}{2}e^{-20(x_1-0.4)^2+(x_2-0.5)^2} \sin(2\pi x_1).$$

We assume that a^\dagger is known on the boundary $\partial\Omega$, and use $H_0^1(\Omega)$ -regularization for a , entering via the adjoint $\tilde{F}'(\cdot)^*$ in (5.10). Note that our chosen ground truth a^\dagger changes its sign around the reference value 1 to avoid simplifications due to monotonicity effects, which are known to act beneficially in parameter identification problems [35, 51].

In this experiment, we vary the noise level and the indenter size to illustrate non-identifiability at the contact shape in the worst case, and feasibility of the reconstruction method and the inverse contact problem in the best case. That is, we choose three different indenters as indicator functions of a circle centered at $(0.5, 0.5)$ with radii

$$\text{indentorradius} \in \{0.1, 0.25, 0.5\} .$$

Furthermore, we vary the relative noise level with

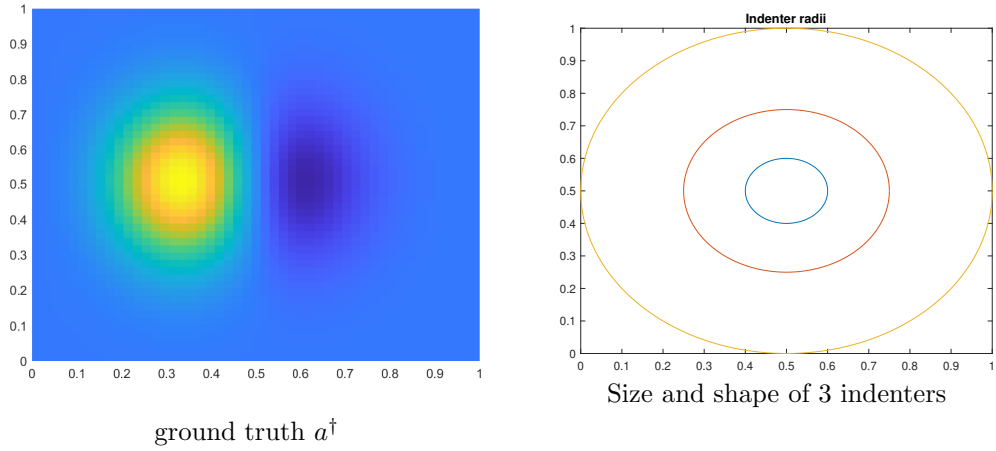
$$\delta_{rel} \in \{0.1\%, 1\%, 10\%\} .$$

To avoid inverse crimes, the noisy data was obtained by first calculating a fine-grid exact solution u and then projecting it onto the calculation grid ($n = 50$). Then, uniformly distributed random noise was added to achieve the desired noise level. In this way, the noise in our data consists of two components: discretization errors and additive noise.

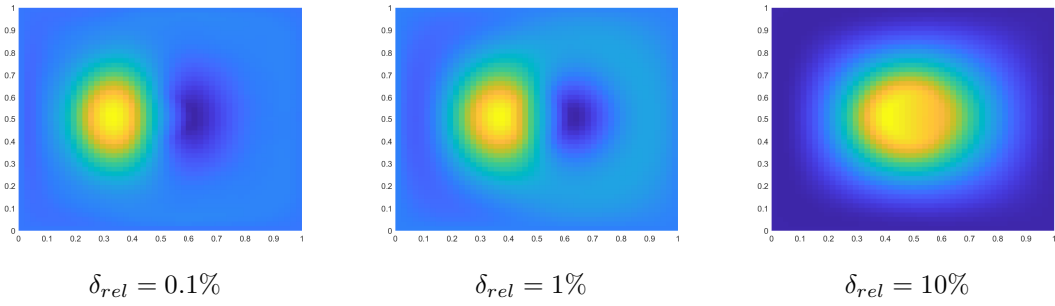
Table 6.2: Experiment 1 with the setup as in Figure 6.3 with different indenter radii: results using (5.10) and, in parenthesis, when using Landweber iteration (5.9).

	rel. err: optimal k $\frac{\ a_{k_{opt}} - a^\dagger\ _{H_0^1}}{\ a^\dagger - 1\ _{H_0^1}}$	rel. err: disrep. princ $\frac{\ a_{k_{disc}} - a^\dagger\ _{H_0^1}}{\ a^\dagger - 1\ _{H_0^1}}$	discrep. factor optimal k $\frac{\ F(a_{k_{opt}}) - y^\delta\ }{\ y - y^\delta\ }$	Stop. index optimal k_{opt}	Stop. index discrepancy k_{disc}
Indenterradius = 0.1					
$\delta = 0.1\%$	0.164 (0.189)	0.222 (0.252)	0.33 (0.56)	381 (>3000)	76 (674)
$\delta = 1\%$	0.457 (0.375)	0.483 (0.500)	0.80 (0.49)	21 (347)	16 (49)
$\delta = 10\%$	0.792 (0.773)	0.793 (0.773)	1.19 (0.97)	1 (2)	2 (2)
Indenterradius = 0.25					
$\delta = 0.1\%$	0.305 (0.314)	0.339 (0.331)	2.10 (0.48)	24 (>3000)	47 (372)
$\delta = 1\%$	0.615 (0.595)	0.692 (0.617)	1.35 (1.32)	7 (14)	10 (23)
$\delta = 10\%$	0.762 (0.761)	1.326 (1.025)	1.10 (1.10)	1 (1)	3 (3)
Indenterradius = 0.5					
$\delta = 0.1\%$	0.819 (0.878)	0.982 (0.984)	0.58 (0.66)	660 (>3000)	13 (30)
$\delta = 1\%$	0.796 (0.793)	0.989 (0.991)	0.82 (0.81)	26 (129)	2 (2)
$\delta = 10\%$	0.801 (0.801)	0.956 (0.956)	0.98 (0.98)	5 (9)	1 (1)

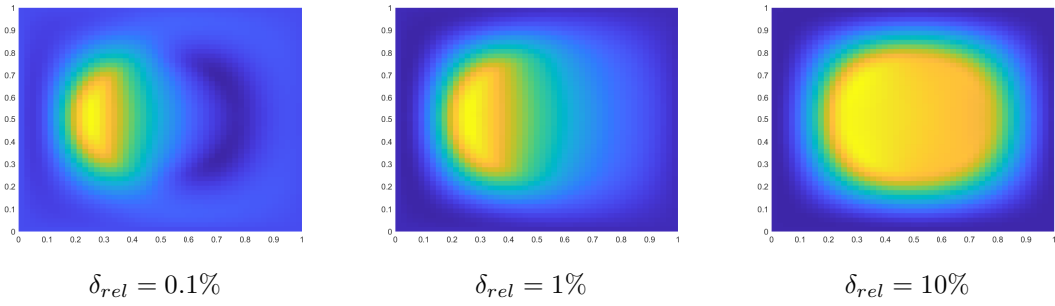
For each combination of indenterradius and noiselevel, we use the iterative method (5.10) as described above with at most $k_{max} = 3000$ iterations. In Figure 6.3, we



Reconstructed a for indenterradius = 0.1



Reconstructed a for indenterradius = 0.25



Reconstructed a for indenterradius = 0.5

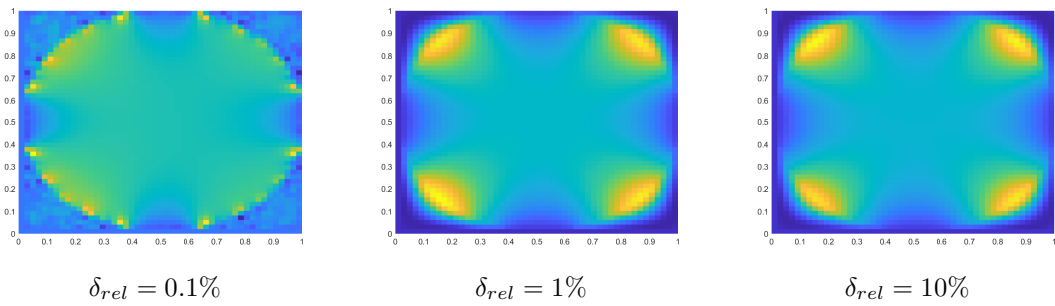


Figure 6.3: Experiment 1: Top: ground truth and 3 different indenter shapes. Results: Left to right: increasing noiselevel: Top to bottom: increasing indenter size.

present the *optimal* result which minimizes $\|a_k - a^\dagger\|_{H_0^1(\Omega)}$ over the iteration index k . Furthermore, in Table 6.2 we present two corresponding error measures, namely

$$\text{relative error} := \frac{\|a_k - a^\dagger\|_{H_0^1(\Omega)}}{\|a^\dagger - 1\|_{H_0^1(\Omega)}}, \quad \text{discrepancy factor} := \frac{\|F(a_k) - y_\delta\|}{\|y - y^\delta\|},$$

both for the optimal case and when the stopping index is determined via the discrepancy principle with the discrepancy factor 1.01. We also performed the same experiments using simple Landweber iteration (5.9), and the results are given in parenthesis.

The conclusions which can be drawn from these results is that the iterative regularization works well with the following expected results: if enough information (small indenter radius) is available, we find good reconstructions for moderate noiselevel ($< 1\%$). In case too little information is available (e.g., for the large indenter, cf. the non-identifiability in Theorem 3.1), then no reasonable reconstruction can be obtained; we again emphasize that this is not a flaw of the method but stems from the problem itself. Compared to simple Landweber iteration, the results are comparable, often better, but with the benefit of a substantial reduction in the required number of iterations.

From Table 6.2, we also observe an unexpected result regarding the discrepancy principle for the optimal stopping rule: the optimal discrepancy index τ_{opt} is in many cases well below 1, which at first contradicts classical theory which requires $\tau \geq 1$. We think that this is related to a non-dense range of the forward operator (non-attainable case): In the linear case, if the forward operator has a non-zero complement in the data space, one should project the residual and the noise onto the closure of the range to get the effective noiselevel and the effective discrepancy principle (see, e.g. [20, p. 84]), otherwise a discrepancy factor below 1 can appear. (This workaround is hardly doable in the nonlinear case, where the range depends on the iteration or on the exact solution.)

Experiment 2. In our second experiment, we illustrate how the constraint can lead to a loss of information and identifiability. For this, we use the same discretization as before, and for the ground-truth a^\dagger we use a sum of two Gaussians of opposite signs, i.e.,

$$a^\dagger(x_1, x_2) := 1 + \frac{1}{2}e^{-20(x_1-0.25)^2+(x_2-0.5)^2} - \frac{1}{2}e^{-20(x_1-0.75)^2+(x_2-0.5)^2}.$$

To test more general setups, we take a non-zero right-hand side $f = 6(x_1(1-x_1) + x_2(1-x_2))$. In this experiment, we use data with random noise $\delta_{\text{rel}} = 0.1\%$, and terminate the after 300 iterations. For the indenter, we select the characteristic function of the thin tall rectangle $[0.45, 0.55] \times [0.1, 0.9]$. Moreover, we consider three different observation setups: i) observation of u on the left part $0 \leq x \leq 0.5$; ii) observation of u on the right part $0.5 \leq x \leq 1$; iii) full observations. See Figure 6.4 (top row) for an illustration, where the ground-truth a^\dagger is displayed together with the indenter shape (yellow dashed lines) and the respective observation region (black lines). The bottom row in Figure 6.4 displays the optimal results after at most 300 iterations. We note that with partial observations, the indenter acts as a kind of barrier for the recovery of the coefficients. Only the part within the observation region can be reconstructed reliably. The result again illustrates the non-uniqueness of the problem, similar to the setup of Figure 3.2.

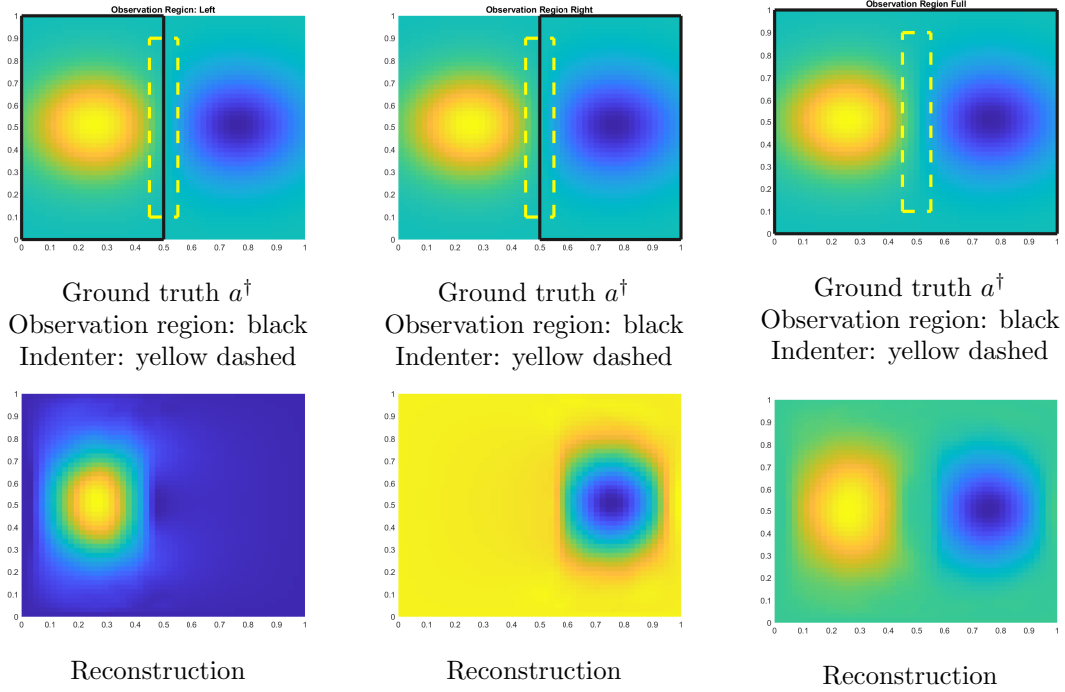


Figure 6.4: Experiment 2: reconstruction from partial observations. Top row: ground truth a^\dagger with indenter region displayed in dashed yellow. The respective observation regions are displayed as rectangles in black. Bottom: reconstruction ($\delta_{rel} = 0.1\%$) (Left: observation on left half; Center: observation on right half; Right: Full observation)

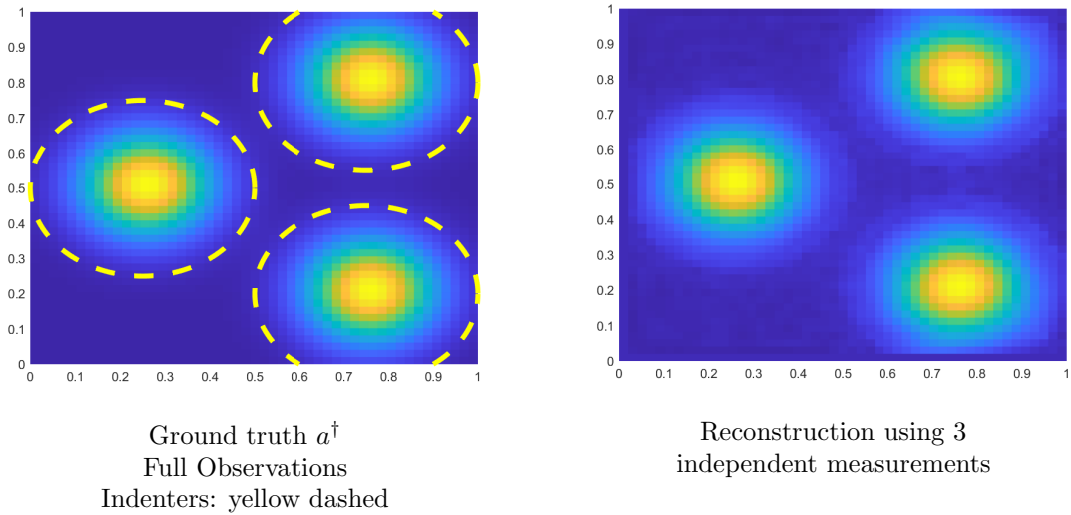


Figure 6.5: Experiment 3: multiple measurements. Left: ground truth and shape of 3 (different) indenters. Right: resulting a_k after $k = 1106$ iterations of method (5.10).

Experiment 3. In our third experiment, we illustrate the benefit of multiple observations in the inverse contact problem. With the same discretization as before, for the

ground-truth a^\dagger we use the sum of three Gaussians centered at three different points:

$$a^\dagger(x_1, x_2) = 1 + 0.5 e^{-50((x_1-0.25)^2+(x_2-0.5)^2)} \\ + 0.5 e^{-50((x_1-0.75)^2+(x_2-0.2)^2)} + 0.5 e^{-50((x_1-0.75)^2+(x_2-0.8)^2)},$$

Also, we choose the same non-zero right-hand side f as Experiment 2. Furthermore, we consider three different, circularly shaped indenters, centered at the same locations as the three Gaussians in the ground-truth a^\dagger , and each with the same radius of 0.25. In this way, each indenter essentially covers one of the Gaussians; see Figure 6.5 (left) for an illustration of the exact solution and the shape of the indenters (yellow dashed).

It is clear that if the indenters are all applied simultaneously, none of the Gaussians of the ground truth can be recovered. However, this is not the case when they are used sequentially: We perform three experiments, where each time only one of the indenters is applied, providing three different solutions u_1, u_2, u_3 . Furthermore, we consider full observations, and thus the data consists of the set $\{u_1, u_2, u_3\}$, contaminated by noise. The noise is added in the same way as in Experiment 1 by using both random and discretization errors with a relative noiselevel of 0.1%. Figure 6.5 (right) illustrates the best iterate obtained within the first 1200 iterations of the Nesterov reconstruction scheme (5.10). We can observe a reasonably accurate reconstruction, which is close to the ground truth. Further experiments not shown here confirm that if only one measurement of u_i is used for reconstruction, then the part of a^\dagger covered by the indenter cannot be reconstructed, while the other two Gaussians can be partially recovered.

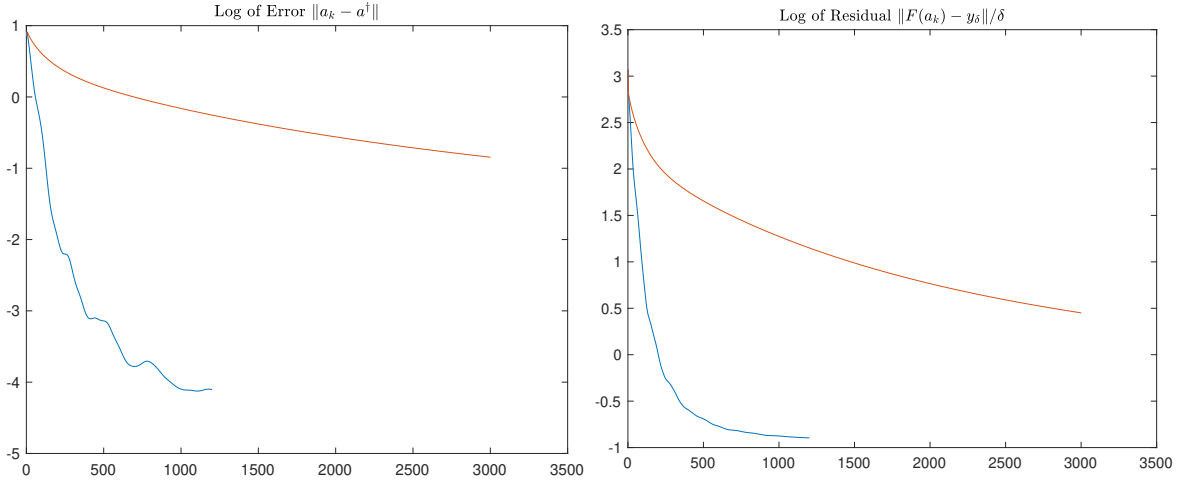


Figure 6.6: Experiment 3: convergence curves for the Nesterov-accelerated reconstruction method (5.10) (blue) and Landweber iteration (5.9) (red) Left: logarithm of error $\|a_k - a^\dagger\|_{H_0^1(\Omega)}$ vs. iterations. Right: logarithm of $\|F(a_k) - y^\delta\| / \|y - y^\delta\|$ vs iterations.

Finally, in Figure 6.6 (left) we display the convergence curves of the log of the error $\|a_k - a^\dagger\|_{H_0^1}$ versus the iteration number k for both the Landweber iteration (5.9) (red) and the Nesterov-accelerated version (5.10) (blue). Furthermore, in Figure 6.6 (right) we display the log of the discrepancy factor $\|F(a_k) - y^\delta\| / \|y - y^\delta\|$ for both methods versus the iteration index k . The acceleration of the Nesterov scheme is clearly visible.

7 Conclusion

In this paper, we considered the identification of a scalar coefficient in a PDE-based parameter estimation problem with contact constraints, serving as an idealized model of a membrane under forces and constrained by a barrier or indenter. We discussed both the forward and inverse parameter estimation problems, as well as uniqueness and non-uniqueness issues caused by the contact constraints. Furthermore, we considered the finite-dimensional versions of these problems, and discussed the design and implementation of corresponding solution and regularization approaches. Finally, we presented a number of numerical experiments demonstrating the performance of our proposed approaches, and illustrating both uniqueness and non-uniqueness situations.

8 Acknowledgements & Support

This research was funded in part by the Austrian Science Fund (FWF) SFB 10.55776/F68 “Tomography Across the Scales”, project F6805-N36 (Tomography in Astronomy) and project F6807-N36 (Tomography with Uncertainties), as well as 10.55776/P34981 “New Inverse Problems of Super-Resolved Microscopy (NIPSUM)”. For open access purposes, the authors have applied a CC BY public copyright license to any author-accepted manuscript version arising from this submission. The financial support by the Austrian Federal Ministry for Digital and Economic Affairs, the National Foundation for Research, Technology and Development and the Christian Doppler Research Association is gratefully acknowledged. The authors thank Prof. Christian Clason, University Graz, for fruitful discussions.

References

- [1] G. Alessandrini. On the identification of the leading coefficient of an elliptic equation. *Boll. Un. Mat. Ital. C (6)*, 4(1):87–111, 1985.
- [2] H. Ammari, E. Bonnetier, Y. Capdeboscq, M. Tanter, and M. Fink. Electrical impedance tomography by elastic deformation. *SIAM Journal on Applied Mathematics*, 68(6):1557–1573, 2008.
- [3] H. Attouch, G. Buttazzo, and G. Michaille. *Variational analysis in Sobolev and BV spaces*, volume 17 of *MOS-SIAM Series on Optimization*. Society for Industrial and Applied Mathematics (SIAM), Philadelphia, PA; Mathematical Optimization Society, Philadelphia, PA, second edition, 2014. Applications to PDEs and optimization.
- [4] G. Bal, F. Monard, and G. Uhlmann. Reconstruction of a fully anisotropic elasticity tensor from knowledge of displacement fields. *SIAM J. Appl. Math.*, 75(5):2214–2231, 2015.
- [5] G. Bal, W. Naetar, O. Scherzer, and J. Schotland. The Levenberg-Marquardt iteration for numerical inversion of the power density operator. *J. Inv. Ill-Posed Problems*, 21(2):265–280, 2013.
- [6] G. Bal and G. Uhlmann. Reconstruction of coefficients in scalar second-order elliptic equations from knowledge of their solutions. *Communications on Pure and Applied Mathematics*, 66(10):1629–1652, 2013.
- [7] H. H. Bauschke and P. L. Combettes. *Convex analysis and monotone operator theory in Hilbert spaces*. Springer, 2017.

- [8] A. Beck. *First-order methods in optimization*, volume 25 of *MOS-SIAM Series on Optimization*. Society for Industrial and Applied Mathematics (SIAM), Philadelphia, PA; Mathematical Optimization Society, Philadelphia, PA, 2017.
- [9] A. Bensaada, E.-H. Essoufi, and A. Zafrar. Primal-dual formulation for parameter estimation in elastic contact problem with friction. *Appl. Math. Sci. Eng.*, 32(1):Paper No. 2367025, 25, 2024.
- [10] M. Bonnet and A. Constantinescu. Inverse problems in elasticity. *Inverse Problems*, 21(2):R1–R50, 2005.
- [11] A. P. Calderón. On an inverse boundary value problem. *Computational & applied mathematics*, 25(2-3):133–138, 2006.
- [12] Y. Capdeboscq, J. Fehrenbach, F. de Gournay, and O. Kavian. Imaging by modification: Numerical reconstruction of local conductivities from corresponding power density measurements. *SIAM Journal on Imaging Sciences*, 2(4):1003–1030, 2009.
- [13] M. Cheney, D. Isaacson, and J. C. Newell. Electrical impedance tomography. *SIAM review*, 41(1):85–101, 1999.
- [14] C. Chicone and J. Gerlach. A note on the identifiability of distributed parameters in elliptic equations. *SIAM J. Math. Anal.*, 18(5):1378–1384, 1987.
- [15] C. Christof and G. Wachsmuth. Differential sensitivity analysis of variational inequalities with locally Lipschitz continuous solution operators. *Appl. Math. Optim.*, 81(1):23–62, 2020.
- [16] C. Christof and G. Wachsmuth. Semismoothness for solution operators of obstacle-type variational inequalities with applications in optimal control. *SIAM J. Control Optim.*, 61(3):1162–1186, 2023.
- [17] C. Clason and V. H. Nhu. Bouligand-Landweber iteration for a non-smooth ill-posed problem. *Numer. Math.*, 142(4):789–832, 2019.
- [18] C. Clason and V. H. Nhu. Bouligand-Landweber iteration for a non-smooth ill-posed problem. *Numer. Math.*, 142(4):789–832, 2019.
- [19] A. Constantinescu and N. Tardieu. On the identification of elastoviscoplastic constitutive laws from indentation tests. *Inverse Problems in Engineering*, 9(1):19–44, 2001.
- [20] H. W. Engl, M. Hanke, and A. Neubauer. *Regularization of inverse problems*. Dordrecht: Kluwer Academic Publishers, 1996.
- [21] H. W. Engl, K. Kunisch, and A. Neubauer. Convergence rates for tikhonov regularisation of non-linear ill-posed problems. *Inverse Problems*, 5(4):523, 1989.
- [22] P. Fernandez-Zelaia, V. J. Roshan, S. R. Kalidindi, and S. N. Melkote. Estimating mechanical properties from spherical indentation using bayesian approaches. *Materials & Design*, 147:92–105, 2018.
- [23] H. Gfrerer. On a globally convergent semismooth* Newton method in nonsmooth nonconvex optimization. *Comp. Optim. Appl.*, 91:67–124, 2025.
- [24] H. Gfrerer, S. Hubmer, and R. Ramlau. On SCD Semismooth* Newton methods for the efficient minimization of Tikhonov functionals with non-smooth and non-convex penalties. *Inverse Problems*, 41(7):075002, 2025. Gold OA.
- [25] H. Gfrerer, M. Mandlmayr, J. V. Outrata, and J. Valdman. On the SCD semismooth* Newton method for generalized equations with application to a class of static contact problems with Coulomb friction. *Comp. Optim. Appl.*, 86:1159–1191, 2022.
- [26] H. Gfrerer and J. V. Outrata. On a semismooth* Newton method for solving generalized equations. *SIAM J. Optim.*, 31(1):489–517, 2021.

- [27] M. S. Gockenbach, B. Jadamba, and A. A. Khan. Equation error approach for elliptic inverse problems with an application to the identification of Lam/’e parameters. *Inverse Problems in Science and Engineering*, 16(3):349–367, 2008.
- [28] M. S. Gockenbach and A. A. Khan. An abstract framework for elliptic inverse problems. I. An output least-squares approach. *Math. Mech. Solids*, 12(3):259–276, 2007.
- [29] M. S. Gockenbach and A. A. Khan. An abstract framework for elliptic inverse problems. II. An augmented Lagrangian approach. *Math. Mech. Solids*, 14(6):517–539, 2009.
- [30] J. Gwinner. An optimization approach to parameter identification in variational inequalities of second kind. *Optim. Lett.*, 12(5):1141–1154, 2018.
- [31] J. Gwinner. An optimization approach to parameter identification in variational inequalities of second kind—II. In *Deterministic and stochastic optimal control and inverse problems*, pages 112–130. CRC Press, Boca Raton, FL, 2022.
- [32] J. Gwinner, B. Jadamba, A. A. Khan, and F. Raciti. *Uncertainty quantification in variational inequalities—theory, numerics, and applications*. CRC Press, Boca Raton, FL, [2022] ©2022.
- [33] J. Gwinner, B. Jadamba, A. A. Khan, and M. Sama. Identification in variational and quasi-variational inequalities. *J. Convex Anal.*, 25(2):545–569, 2018.
- [34] M. Hanke, A. Neubauer, and O. Scherzer. A convergence analysis of the Landweber iteration for nonlinear ill-posed problems. *Numerische Mathematik*, 72(1):21–37, 1995.
- [35] B. Harrach and M. Ullrich. Monotonicity-based shape reconstruction in electrical impedance tomography. *SIAM J. Math. Anal.*, 45(6):3382–3403, 2013.
- [36] B. Hofmann, B. Kaltenbacher, C. Pöschl, and O. Scherzer. A convergence rates result for Tikhonov regularization in Banach spaces with non-smooth operators. *Inverse Problems*, 23(3):987–1010, 2007.
- [37] D. Holder and A. Adler. *Electrical impedance tomography: methods, history and applications*. Series in medical physics and biomedical engineering. CRC Press, second edition edition, 2022.
- [38] S. Hubmer, K. Knudsen, C. Li, and E. Sherina. Limited-angle acousto-electrical tomography. *Inverse Problems in Science and Engineering*, 27(9):1298–1317, 2019.
- [39] S. Hubmer and R. Ramlau. Convergence analysis of a two-point gradient method for nonlinear ill-posed problems. *Inverse Problems*, 33(9):095004, 2017.
- [40] S. Hubmer, E. Sherina, and R. Ramlau. Characterizations of adjoint Sobolev embedding operators with applications in inverse problems. *Electron. Trans. Numer. Anal.*, 59:116–144, 2023.
- [41] V. Isakov. *Inverse Problems for Partial Differential Equations*. Applied Mathematical Sciences. Springer, New York, NY, 2006.
- [42] B. Jadamba, A. A. Khan, F. Raciti, and M. Sama. A variational inequality based stochastic approximation for estimating the flexural rigidity in random fourth-order models. *Commun. Nonlinear Sci. Numer. Simul.*, 111:Paper No. 106406, 11, 2022.
- [43] Q. Jin and Y. Zhang. Bouligand-Newton type methods for non-smooth ill-posed problems. *Inverse Problems*, 40(10):Paper No. 105011, 28, 2024.
- [44] B. Kaltenbacher. Regularization based on all-at-once formulations for inverse problems. *SIAM J. Numer. Anal.*, 54(4):2594–2618, 2016.
- [45] B. Kaltenbacher. Minimization based formulations of inverse problems and their regularization. *SIAM J. Optim.*, 28(1):620–645, 2018.

- [46] B. Kaltenbacher, A. Kirchner, and B. Vexler. Goal oriented adaptivity in the IRGNM for parameter identification in PDEs: II. all-at-once formulations. *Inverse Problems*, 30(4):045002, 33, 2014.
- [47] B. Kaltenbacher, A. Neubauer, and O. Scherzer. *Iterative regularization methods for nonlinear ill-posed problems*. Berlin: de Gruyter, 2008.
- [48] B. Kaltenbacher, F. Schöpfer, and T. Schuster. Iterative methods for nonlinear ill-posed problems in Banach spaces: convergence and applications to parameter identification problems. *Inverse Problems*, 25(6):065003 (19pp), 2009.
- [49] A. A. Khan and D. Motreanu. Inverse problems for quasi-variational inequalities. *J. Global Optim.*, 70(2):401–411, 2018.
- [50] N. Kikuchi and J. T. Oden. *Contact problems in elasticity: a study of variational inequalities and finite element methods*, volume 8 of *SIAM Studies in Applied Mathematics*. Society for Industrial and Applied Mathematics (SIAM), Philadelphia, PA, 1988.
- [51] S. Kindermann. On the tangential cone condition for electrical impedance tomography. *Electron. Trans. Numer. Anal.*, 57:17–34, 2022.
- [52] R. V. Kohn and M. Vogelius. Relaxation of a variational method for impedance computed tomography. *Comm. Pure Appl. Math.*, 40(6):745–777, 1987.
- [53] Y. Ma, F. Liu, Z. Si, Q. Gerile, K. Yang, H. Li, and Y. Cheng. Parameter identification of contact model for tank saddle ring system based on genetic algorithm and bp neural network. *Journal of Physics: Conference Series*, 2478(12):122017, jun 2023.
- [54] J. Mueller and S. Siltanen. *Linear and Nonlinear Inverse Problems with Practical Applications*. Society for Industrial and Applied Mathematics, Philadelphia, PA, 2012.
- [55] Y. Nesterov. A method of solving a convex programming problem with convergence rate $O(1/k^2)$. *Soviet Mathematics Doklady*, 27(2):372–376, 1983.
- [56] J. Radová and J. Machalová. Parameter identification in contact problems for Gao beam. *Nonlinear Anal. Real World Appl.*, 77:Paper No. 104068, 22, 2024.
- [57] A.-T. Rauls and G. Wachsmuth. Generalized derivatives for the solution operator of the obstacle problem. *Set-Valued Var. Anal.*, 28(2):259–285, 2020.
- [58] G. R. Richter. An inverse problem for the steady state diffusion equation. *SIAM J. Appl. Math.*, 41(2):210–221, 1981.
- [59] A. Rieder. On the regularization of nonlinear ill-posed problems via inexact Newton iterations. *Inverse Problems*, 15(1):309–327, 1999.
- [60] T. Sahin, M. von Danwitz, and A. Popp. Solving forward and inverse problems of contact mechanics using physics-informed neural networks. *Advanced Modeling and Simulation in Engineering Sciences*, 11:Paper No. 11, 30, 2024.
- [61] O. Scherzer, M. Grasmair, H. Grossauer, M. Haltmeier, and F. Lenzen. *Variational methods in imaging*, volume 167 of *Applied Mathematical Sciences*. Springer, New York, 2009.
- [62] C. Sun, Q. Lin, B. Wang, J. Huang, and J. Chen. Modeling and inverse identification method for the characterization of elastic-plastic contact behavior during flat punch indentation. *Eur. J. Mech. A Solids*, 96:Paper No. 104663, 15, 2022.
- [63] N. Tardieu and A. Constantinescu. On the determination of elastic coefficients from indentation experiments. *Inverse Problems*, 16(3):577–588, 2000.
- [64] H. Zhang and L. V. Wang. Acousto-electric tomography. In *Proceedings SPIE, Photons Plus Ultrasound: Imaging and Sensing*, 5320(9), page 145, 2004.